

Moving doubly heavy baryon in a strongly coupled plasma from holography*

Xuan Liu (刘旋)¹ Jia-Jie Jiang (江佳杰)¹ Xun Chen (陈勋)^{1†} Mitsutoshi Fujita^{1‡} Akira Watanabe^{2§}

¹School of Nuclear Science and Technology, University of South China, Hengyang 421001, China

²School of Mathematics and Physics, University of South China, Hengyang 421001, China

Abstract: Gauge/gravity duality is used to study properties of the doubly heavy baryon (QQq) at finite rapidity and temperature in the heavy-ion collision. We investigate the impact of rapidity on string breaking and screening of QQq, and compare these effects with the results for Q \bar{Q} in detail. Computations reveal that the string-breaking distances of QQq and Q \bar{Q} are close in the confined state and the effects of rapidity and temperature on the string breaking are not significant. An interesting result shows that QQq cannot be found at high enough temperatures and rapidities; however, Q \bar{Q} can exist under any conditions as long as the separation distance is small enough. Besides, the screening distances of QQq and Q \bar{Q} are also compared at finite rapidity and temperature. Based on the above analysis, we infer that Q \bar{Q} is more stable than QQq at finite rapidity and temperature.

Keywords: holographic QCD, QGP, heavy quark

DOI:

I. INTRODUCTION

In the recent LHCb experiment at CERN, researchers have made an exciting discovery of a particle known as Ξ_{cc}^{++} [1, 2]. This groundbreaking finding has sparked significant interest in the exploration of double charm baryons. The Ξ_{cc}^{++} particle is formed by the combination of two heavy quarks with a single light quark, resulting in a highly distinctive structure. In this study, we adopt an assumption of potential models, which suggests that the interaction between heavy quarks and anti-quarks within hadrons can be described by a potential energy [3].

While lattice gauge theory remains a fundamental tool for studying non-perturbative phenomena in Quantum Chromodynamics (QCD), its investigation of the doubly heavy baryon potential has been relatively limited so far [4, 5]. On the other hand, gauge/gravity duality provides a new theoretical tool for studying strongly coupled gauge theories, and in Ref. [6], the holographic potential of quark-antiquark pairs was computed for the first time. Based on the study in Ref. [6], the potential was further investigated in Refs. [7, 8] to study the potential at finite temperature. In recent years, the methodology of utilizing holographic theories to study multi-quark potentials

has been increasingly refined. The obtained multi-quark potentials from holography are in good agreement with lattice calculations and QCD phenomenology [9–20]. The techniques employed to extract the QQq potential in our study are analogous to those used in lattice QCD [21].

The creation of quark-gluon plasma (QGP) through high-energy heavy-ion collisions allows us to simulate the high temperature and density conditions of the early universe [22–25]. The formation of this QGP is crucial for our understanding of the early stages of cosmic evolution and the fundamental properties of quark color dynamics. At low temperatures, quarks and gluons are confined within hadrons. As the separation between quarks increases, the strong interaction force becomes stronger. When the separation reaches a limit, new quark-anti-quark pairs are typically produced, resulting in the confinement of quarks within hadrons. This behavior is manifested as string breaking in this study. Under extreme conditions, the strong interaction between hadrons diminishes at long range, allowing quarks to move freely over larger distances [26–28].

In heavy-ion collision experiments, heavy ions collide at speeds close to the speed of light, forming QGP [25]. Similar to the early universe, this substance does not

Received 29 January 2024; Accepted 3 April 2024

* This work is supported by the Natural Science Foundation of Hunan Province of China under Grant No. 2022JJ40344, and the Research Foundation of Education Bureau of Hunan Province, China (Grant No. 21B0402)

[†] E-mail: chenxunhep@qq.com

[‡] E-mail: fujitamitsutoshi@usc.edu.cn

[§] E-mail: watanabe@usc.edu.cn



Content from this work may be used under the terms of the Creative Commons Attribution 3.0 licence. Any further distribution of this work must maintain attribution to the author(s) and the title of the work, journal citation and DOI. Article funded by SCOAP³ and published under licence by Chinese Physical Society and the Institute of High Energy Physics of the Chinese Academy of Sciences and the Institute of Modern Physics of the Chinese Academy of Sciences and IOP Publishing Ltd

remain stationary but rapidly expands. Therefore, when studying the doubly heavy baryon, the effect of rapidity must be considered. This is crucial for understanding the interaction between QQq and the medium, as well as the transport properties within the QGP. By studying the behavior of moving QQq, more comprehensive information about the QGP can be obtained, leading to further investigation into the properties of QCD. By studying the variation of string breaking under different temperature and rapidity conditions, we can study decay rates of different hadrons in different conditions[29].

Gauge/gravity duality was initially proposed by Maldacena [30] for conformal field theories, and later extended to include theories resembling QCD, establishing a connection between string theory and heavy-ion collisions in some manner [31–33]. The study of moving heavy quarkonium can be found in Refs. [34–50].

The remaining sections of this paper are as follows: In Sec. II, we will construct string configurations considering the effects of finite temperature and finite rapidity. In Sec. III, we will discuss the computation of the model's potential energy. At first, we calculate the influence of rapidity on the string breaking of QQq. Then, we discuss its screening and provide a comprehensive comparison with $Q\bar{Q}$. Additionally, we also plot their state diagram in the $T-\eta$ plane. Finally, we summarize these findings in Sec. IV.

II. MODEL SETUP

First, the background metric at a finite temperature is given as [13, 14, 51–53]:

$$ds^2 = w(r) \left(-f(r)dt^2 + d\vec{x}^2 + \frac{1}{f(r)}dr^2 \right) + e^{-sr^2} g_{ab}^{(5)} d\omega^a d\omega^b, \quad (1)$$

where

$$\begin{aligned} w(r) &= \frac{e^{sr^2} R^2}{r^2}, \\ f(r) &= 1 - \frac{r^4}{r_h^4}. \end{aligned} \quad (2)$$

The metric represents a one-parameter deformation of Euclidean $AdS_5 \times S_5$ space, parametrized by s and with a radius R . It consists of a five-dimensional compact space (sphere) X with coordinates ω^a , a blackening factor $f(r)$, and a black hole horizon (brane) at r_h . The Hawking temperature of the black hole T is defined as follows:

$$T = \frac{1}{4\pi} \left| \frac{df}{dr} \right|_{r=r_h} = \frac{1}{\pi r_h}. \quad (3)$$

In this work, we investigate the motion of a particle

consisting of two heavy quarks and one light quark in a thermal medium. We divide the particle's spatial coordinates into three directions: x_1 (connecting the heavy quark pair), x_2 , and x_3 (perpendicular to the heavy quark pair). We find that the coefficients of x_1 and x_2 in the metric are the same, which implies that the presence of the heavy quark pair at either x_1 or x_2 does not affect the calculation results. Due to the temperature and rapidity being constant, we can consider the doubly heavy baryon to be in a state of force equilibrium. Furthermore, energy loss has not been taken into account in this paper, which can be discussed in future work.

In our study, we consider where the QQq is moving with a constant rapidity η along the x_3 direction [34–36, 43, 46]. For convenience, let us consider a new scenario in which the QQq is at rest, while the surrounding medium is in motion relative to it. We then introduce the Lorentz transform to reflect the effect of rapidity η on it and obtain the new metric:

$$\begin{aligned} ds^2 &= w(r) \left(-g_1(r)dt^2 - 2 \sinh(\eta) \cosh(\eta) \left(1 - \frac{g_1(r)}{g_2(r)} \right) dx_3 dt \right. \\ &\quad \left. + g_3(r) dx_3^2 + dx_1^2 + dx_2^2 + \frac{g_2(r)}{g_1(r)} dr^2 \right) + e^{-sr^2} g_{ab}^{(5)} d\omega^a d\omega^b, \end{aligned} \quad (4)$$

where

$$\begin{aligned} g_1(r) &= f(r) \cosh^2(\eta) - \sinh^2(\eta), \\ g_2(r) &= \frac{g_1(r)}{f(r)}, \\ g_3(r) &= \cosh^2(\eta) - f(r) \sinh^2(\eta). \end{aligned} \quad (5)$$

The Nambu-Goto action of a string is

$$S_{NG} = -\frac{1}{2\pi\alpha'} \int d\xi^0 d\xi^1 \sqrt{-\det g_{ab}}, \quad (6)$$

where α' is a constant, (ξ^0, ξ^1) are worldsheet coordinates, and g_{ab} is an induced metric. We introduce the baryon vertex and heavy and light quarks to construct the QQq configuration. Then we know from AdS/CFT that the vertex is a five brane [54, 55]. At leading order in α' , the baryon vertex action is $S_{vert} = \tau_5 \int d^6 \xi \sqrt{\gamma^{(6)}}$, where τ_5 is the brane tension and ξ^i is the worldvolume coordinates. Since the brane is wrapped on the X interior space, it looks point-like in AdS_5 . We choose a static gauge $\xi^0 = t, \xi^a = \theta^a$ with θ^a is the coordinates on X . So, the action is

$$S_{vert} = \tau_v \int dt \frac{e^{-2sr^2}}{r} \sqrt{g_1(r)}, \quad (7)$$

where τ_v is a dimensionless parameter defined by

$\tau_v = \tau_5 R \text{vol}(X)$ and $\text{vol}(X)$ is a volume of X .

Finally, we consider the light quark at the end of the string as a tachyon field, which couples to the worldsheet boundary by $S_q = \int d\tau e T$ [56, 57]. This term is typical for strings propagating in an open string tachyon background and T is its background scalar [56]. The integral is over a worldsheet boundary parameterized by τ and e represents the boundary metric. In this paper, we can assume T to be a constant T_0 , and the integral reduces to a coordinate integral of t . Thus, the action can be given as

$$S_q = m \int dt \frac{e^{\frac{sr^2}{2}}}{r} \sqrt{g_1(r)}, \quad (8)$$

where $m = RT_0$. This represents a particle with a mass T_0 is at rest, while the surrounding medium with a temperature T moves relative to it with a rapidity η . The parameters we select are as follows: $g = \frac{R^2}{2\pi\alpha'} = 0.176$, $k = \frac{\tau_v}{3g} = -0.321$, $n = \frac{m}{g} = 3.057$, $s = 0.45 \text{ GeV}^2$, $c = 0.623 \text{ GeV}$ [20].

A. Small L

As shown in Fig. 1, the heavy quark pair, light quark, and baryon vertex are connected by three strings, with the separation distance between the heavy quark pair de-

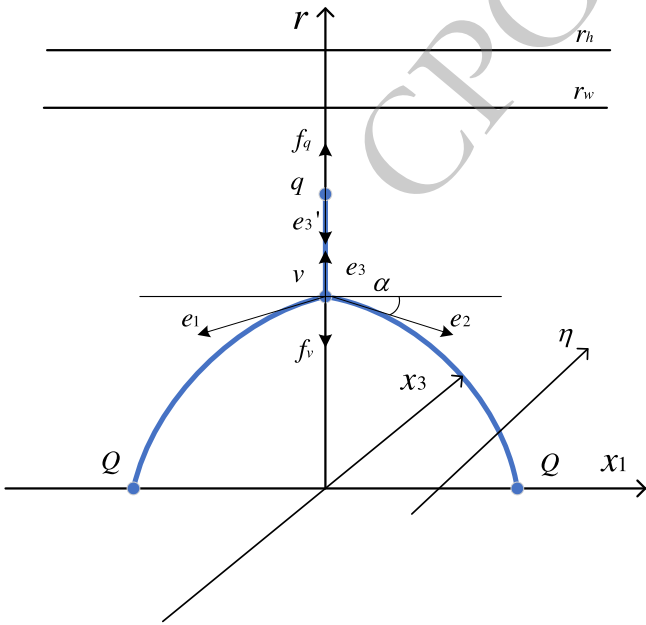


Fig. 1. (color online) A string configuration at a small separation distance of heavy quark pair. We use the line connecting two heavy quarks Q as the x_1 -axis, while the baryon vertex v and the light quark q are on the r -axis. The rapidity η is along the x_3 -axis direction. The heavy quark, light quark, and baryon vertex are connected by blue strings. The black arrows represent generalized forces. r_h is the position of the black hole horizon. r_w is the position of an imaginary wall when the QQq is confined.

noted as L . Therefore, we can express the total action as follows:

$$S = \sum_{i=1}^3 S_{NG}^{(i)} + S_{vert} + S_q. \quad (9)$$

According to the previous discussion, since the results obtained from x_1 and x_2 are the same, we directly designate the line where the heavy quark pair is located as x_1 , and the rapidity perpendicular to the x_1 direction as x_3 , as shown in Fig. 1. Hereafter, we refer to x_1 as x . Then, in this configuration, we choose the static gauge where $\xi^0 = t$, $\xi^1 = r$, and consider x as a function of r . Therefore, the total sum of the Nambu-Goto action can be written as:

$$\sum_{i=1}^3 S_{NG}^{(i)} = 2g \int_0^t dt \int_0^{r_v} w(r) \sqrt{g_1(r)(\partial_r x)^2 + g_2(r)} dr + g \int_0^t dt \int_{r_v}^{r_q} w(r) \sqrt{g_1(r)(\partial_r x)^2 + g_2(r)} dr, \quad (10)$$

where $\partial_r x = \frac{\partial x}{\partial r}$ and $x(r)$ satisfies the following boundary conditions:

$$\begin{cases} x(0) = \pm \frac{L}{2}, x(r_v) = x(r_q) = 0, \\ \begin{cases} (\partial_r x)^2 = \cot^2(\alpha), & r = r_v \\ (\partial_r x)^2 = 0, & r \in (r_v, r_q]. \end{cases} \end{cases} \quad (11)$$

Now, we combine the baryon vertex and the light quark to write that the total action is

$$\begin{aligned} S = & gt \left(2 \int_0^{r_v} w(r) \sqrt{g_1(r)(\partial_r x)^2 + g_2(r)} dr \right. \\ & + \int_{r_v}^{r_q} w(r) \sqrt{g_2(r)} dr \\ & \left. + 3k \frac{e^{-2sr^2}}{r} \sqrt{g_1(r)} + n \frac{e^{\frac{sr^2}{2}}}{r} \sqrt{g_1(r)} \right). \end{aligned} \quad (12)$$

It is easy to find that the first term is divergent, so we get the potential energy according to $E = S/t$ after normalization

$$\begin{aligned} E_{QQq} = & g \left(2 \int_0^{r_v} \left(w(r) \sqrt{g_1(r)(\partial_r x)^2 + g_2(r)} - \frac{1}{r^2} \right) dr - \frac{2}{r_v} \right. \\ & + \int_{r_v}^{r_q} w(r) \sqrt{g_2(r)} dr \\ & \left. + 3k \frac{e^{-2sr^2}}{r_v} \sqrt{g_1(r_v)} + n \frac{e^{\frac{sr^2}{2}}}{r_q} \sqrt{g_1(r_q)} \right) + 2c. \end{aligned} \quad (13)$$

With r_v as the independent variable at fixed T and η . By substituting the first term of the unnormalized energy into the Euler-Lagrange equation, we obtain:

$$\mathcal{H} = \frac{w(r)g_1(r)\partial_r x}{\sqrt{g_1(r)(\partial_r x)^2 + g_2(r)}}, \quad (14)$$

since \mathcal{H} is a constant, we have:

$$\mathcal{H}|_{r=r_v} = \frac{w(r_v)g_1(r_v)\cot(\alpha)}{\sqrt{g_1(r_v)\cot^2(\alpha) + g_2(r_v)}}. \quad (15)$$

According to $\mathcal{H} = \mathcal{H}|_{r=r_v}$,

$$\begin{aligned} \partial_r x = & \\ & \sqrt{\frac{w(r_v)^2 g_1(r_v)^2 g_2(r)}{w(r)^2 g_1(r)^2 (g_1(r_v) + g_2(r_v) \tan^2(\alpha)) - g_1(r) w(r_v)^2 g_1(r_v)^2}}. \end{aligned} \quad (16)$$

Now we need to determine the position of the light quark r_q and the angle α between the string and the x -axis at the baryon vertex. The generalized force equilibrium equations at the baryon vertex and the light quark must be equal to zero. First, we take the variation of their respective action quantities to obtain their generalized forces:

$$e_1 = gw(r_v) \left(-\sqrt{\frac{g_1(r_v)f(r_v)}{f(r_v) + \tan^2 \alpha}}, -\sqrt{\frac{g_1(r_v)}{f(r_v)^2 \cot^2(\alpha) + f(r_v)}} \right), \quad (17)$$

$$e_2 = gw(r_v) \left(\sqrt{\frac{g_1(r_v)f(r_v)}{f(r_v) + \tan^2 \alpha}}, -\sqrt{\frac{g_1(r_v)}{f(r_v)^2 \cot^2(\alpha) + f(r_v)}} \right), \quad (18)$$

$$e_3 = gw(r_v) (0, \sqrt{g_2(r_v)}), \quad (19)$$

$$e'_3 = gw(r_q) (0, -\sqrt{g_2(r_q)}), \quad (20)$$

$$f_q = \left(0, -gn\partial_{r_q} \left(\frac{e^{\frac{sr_q^2}{2}}}{r_q} \sqrt{g_1(r_q)} \right) \right), \quad (21)$$

$$f_v = \left(0, -3gk\partial_{r_v} \left(\frac{e^{-2sr_v^2}}{r_v} \sqrt{g_1(r_v)} \right) \right), \quad (22)$$

where e_i is the string tension, and f_q and f_v are the forces provided by the light quark and baryon vertices, respectively [20].

It is evident that the generalized force equilibrium equation at the light quark is solely a function of r_q and can be expressed as follows:

$$F_1(r_q) = \frac{f_q + e'_3}{gw(r_q)} = 0. \quad (23)$$

In addition, we can also solve for r_q based on this equation by changing T and η . The force balance equation at the vertex is:

$$f_v + e_3 + e_1 + e_2 = 0. \quad (24)$$

In addition to T and η , the equation has only two unknowns, r_v , and α . By solving the equation, we can obtain the function of α as a function of r_v . Then we can give the distance L as a function of r_v :

$$L = 2 \int_0^{r_v} \frac{\partial x}{\partial r} dr. \quad (25)$$

Together with Eqs. (13) and (25), we can numerically solve the energy at small L .

B. Intermediate L

According to Fig. 2, compared to small L , intermediate L is only missing a straight string from r_v to r_q , and the sum of the action can be written as

$$S = \sum_{i=1}^2 S_{NG}^{(i)} + S_{vert} + S_q. \quad (26)$$

We still chose the same static gauge as before. It is easy to know that the sum of Nambu-Goto action becomes

$$\sum_{i=1}^2 S_{NG}^{(i)} = 2g \int_0^t dt \int_0^{r_v} w(r) \sqrt{g_1(r)(\partial_r x)^2 + g_2(r)} dr. \quad (27)$$

Then the boundary condition becomes

$$x(0) = \pm \frac{L}{2}, x(r_v) = 0, (\partial_r x|_{r=r_v})^2 = \cot^2(\alpha). \quad (28)$$

Therefore, the potential energy is

$$\begin{aligned} E_{QQq} = & g \left(2 \int_0^{r_v} (w(r) \sqrt{g_1(r)(\partial_r x)^2 + g_2(r)} - \frac{1}{r^2}) dr - \frac{2}{r_v} \right. \\ & \left. + 3k \frac{e^{-2sr_v^2}}{r_v} \sqrt{g_1(r_v)} + n \frac{e^{\frac{sr_q^2}{2}}}{r_v} \sqrt{g_1(r_v)} \right) + 2c. \end{aligned} \quad (29)$$

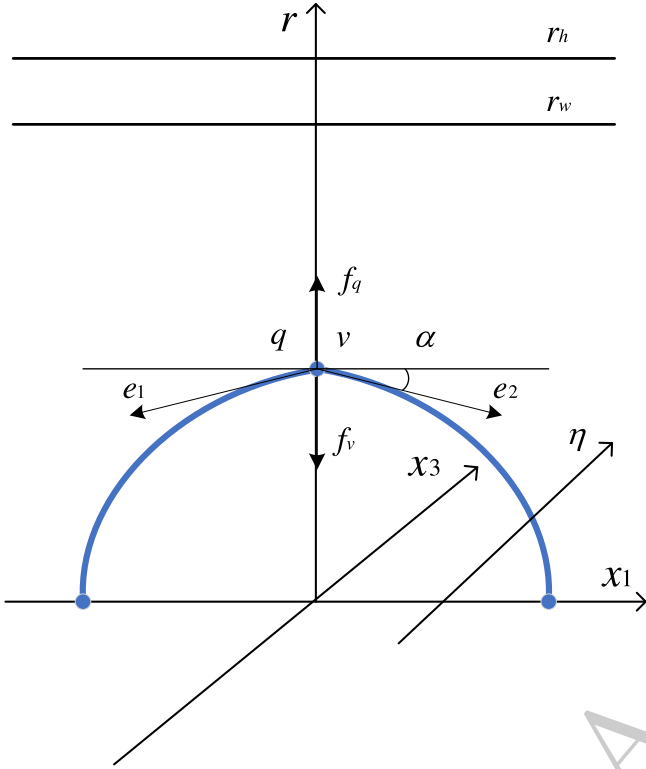


Fig. 2. (color online) A string configuration at an intermediate separation distance of a heavy quark pair. We use the straight line between two heavy quarks Q as the x_1 -axis, and baryon vertex and light quarks are in the same position on the r -axis. The rapidity η is along the x_3 -axis direction. The black arrows represent generalized forces. r_h is the position of the black hole horizon. r_w is the position of an imaginary wall when the QQq is confined.

Finally, we can write the equation for the equilibrium of generalized force at the coincidence of the light quark and the baryon vertex as

$$f_v + f_q + e_1 + e_2 = 0, \quad (30)$$

and each force is given by

$$e_1 = gw(r_v) \left(-\sqrt{\frac{g_1(r_v)f(r_v)}{f(r_v) + \tan^2 \alpha}}, -\sqrt{\frac{g_1(r_v)}{f(r_v)^2 \cot^2(\alpha) + f(r_v)}} \right), \quad (31)$$

$$e_2 = gw(r_v) \left(\sqrt{\frac{g_1(r_v)f(r_v)}{f(r_v) + \tan^2 \alpha}}, -\sqrt{\frac{g_1(r_v)}{f(r_v)^2 \cot^2(\alpha) + f(r_v)}} \right), \quad (32)$$

$$f_q = \left(0, -gn\partial_{r_v} \left(\frac{e^{-\frac{sr_v^2}{2}}}{r_v} \sqrt{g_1(r_v)} \right) \right), \quad (33)$$

$$f_v = \left(0, -3gk\partial_{r_v} \left(\frac{e^{-2sr_v^2}}{r_v} \sqrt{g_1(r_v)} \right) \right). \quad (34)$$

According to Eqs. (25) and (29), we can obtain the energy at intermediate L .

C. Large L

As can be seen from Fig. 3, the configuration still consists of two strings, the vertex, and the light quark. However, due to the presence of smooth turning points on the strings, we can utilize a new static gauge that simplifies the calculations. In this gauge, we set $\xi^0 = t$, $\xi^1 = x$, and consider r as a function of x now. Accordingly, we can express the total action as follows:

$$S = gt \left(\int_{-\frac{L}{2}}^0 w(r) \sqrt{g_1(r) + g_2(r)} (\partial_x r)^2 dx + \int_0^{\frac{L}{2}} w(r) \sqrt{g_1(r) + g_2(r)} (\partial_x r)^2 dx + 3k \frac{e^{-2sr^2}}{r} \sqrt{g_1(r)} + n \frac{e^{\frac{sr^2}{2}}}{r} \sqrt{g_1(r)} \right). \quad (35)$$

And now the boundary condition of $r(x)$ is

$$r\left(\pm \frac{L}{2}\right) = 0, \quad r(0) = r_v, \quad \begin{cases} (\partial_x r)^2 = \tan^2(\alpha), & r = r_v \\ (\partial_x r)^2 = 0, & r = r_0. \end{cases} \quad (36)$$

The generalized force balance equation at r_v is the same as for intermediate L . We can use this equation to relate r_v to α . Additionally, we need to find the functional relationship between r_0 and r_v due to inflection points. To accomplish this, we can employ the Euler-Lagrange equation and incorporate the action of the string to derive the first integral.

$$\mathcal{H} = \frac{w(r)g_1(r)}{\sqrt{g_1(r) + g_2(r)} (\partial_x r)^2}, \quad (37)$$

\mathcal{H} is a constant. We bring the boundary conditions to the first integral.

$$\mathcal{H}|_{r=r_v} = \frac{w(r_v)g_1(r_v)}{\sqrt{g_1(r_v) + g_2(r_v)} \tan^2(\alpha)}, \quad (38)$$

$$\mathcal{H}|_{r=r_0} = w(r_0) \sqrt{g_1(r_0)}. \quad (39)$$

So we obtain

$$\partial_x r = \sqrt{\frac{w(r)^2 g_1(r)^2 - g_1(r) w(r_0)^2 g_1(r_0)}{w(r_0)^2 g_1(r_0) g_2(r)}}. \quad (40)$$

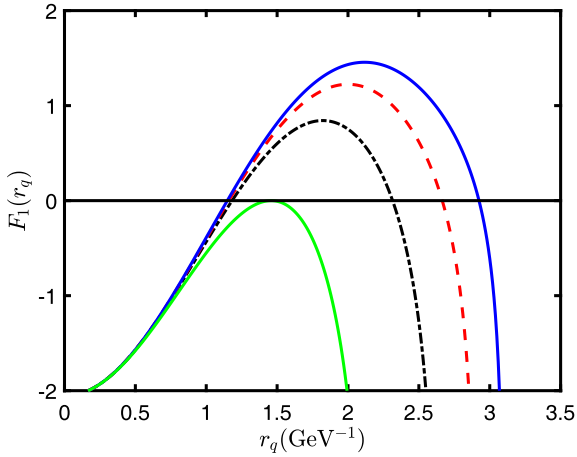


Fig. 4. (color online) F_1 as a function of r_q for various rapidities at $T = 0.1 \text{ GeV}$. The blue line represents $\eta = 0.3$; the red dashed line represents $\eta = 0.6$; the black dot-dashed line represents $\eta = 0.9$; the green line represents $\eta = 1.3865$. Only the green line has one zero point, and the other three lines have two zero points.

We calculate the angle at different rapidities using Eq. (24), as a function of r_v at a temperature of $T = 0.1 \text{ GeV}$. The resulting plot is shown in Fig. 5. It is evident that regardless of the parameters, the angles are always greater than zero, and as the rapidity increases, the angle decreases. The transverse axes of the angles all start at zero and end at their respective light quark positions r_q . When the baryon vertex coincides with the light quark, denoted by $r_v = r_q$, it indicates that the configuration has entered the second stage, which is the intermediate L . Subsequently, the light quark and the baryon vertex rise together. The stage where $r_v < r_q$ is referred to as the first stage, known as the small L .

At the intermediate L , we can solve Eq. (30) to obtain the relation between the angles α and r_v . Then we draw this plot at different rapidities, as shown in Fig. 6. It can be seen that when the rapidity is small, the angle decreases with r_v linearly, and when it decreases to less than 0, we consider that QQq transitions from the second stage to the third stage, which is large L . In addition, as the rapidity increases, the angular plot of the second stage changes greatly. The curve of α always moves upwards, no longer monotonically decreasing, and it gradually bends upwards from a straight line to a curve, ultimately becoming monotonically increasing. From the results, when the rapidity is large, the third stage configuration of the model will not be possible.

Fig. 7 shows the relation between the angles α and the r_v in the third stage. This result is obtained through Eq. (30). Their transverse axes all start at the end point of their respective second stages, and the longitudinal axes start at 0. It can be seen that as the rapidity increases, the range of configuration in the third stage continues to de-

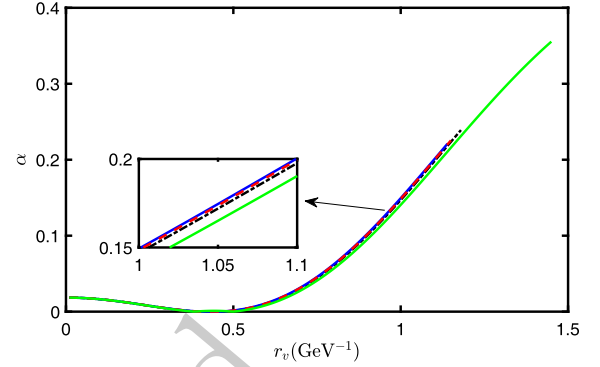


Fig. 5. (color online) The relation between the position r_v of the baryon vertex and the angle α , which is between the string and the horizon, at $T = 0.1 \text{ GeV}$ and various rapidities. Among them, the blue line represents $\eta = 0.3$; the red dashed line represents $\eta = 0.6$; the black dot-dashed line represents $\eta = 0.9$; the green line represents $\eta = 1.3865$.

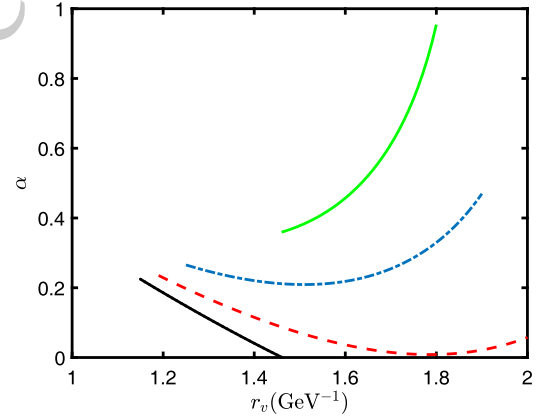


Fig. 6. (color online) The relation between the position r_v of the baryon vertex and the angle α , which is between the string and the horizontal, at $T = 0.1 \text{ GeV}$ and various rapidities. Among them, the black line represents $\eta = 0.3$; the red dashed line represents $\eta = 0.9$; the blue dot-dashed line represents $\eta = 1.2$; the green line represents $\eta = 1.3865$.

crease until it no longer exists. This dovetails with our analysis in the second phase. Since the string configuration features smooth turning points during the third stage, we obtain the relation between r_v and r_0 using Eq. (41), as shown in Fig. 8. From the calculated results between α and r_v in each stage, it can be observed that α is smooth between the two stages.

In Fig. 9, we present the results of L as a function of r_v based on Eqs. (25) and (43). At $T = 0.1 \text{ GeV}$, $\eta = 0.3$, the QQq will be confined and the separation distance can tend to infinity. Subsequently, we use Eqs. (13), (29), and (42) to obtain a plot of E and L as shown in Fig. 10. In the confined state, the potential of QQq is also the Cornell potential with finite temperature and rapidity.

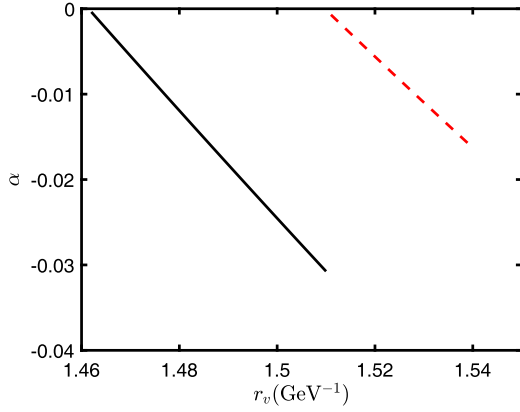


Fig. 7. (color online) The relation between the position r_v of the baryon vertex and the angle α , which is between the string and the horizontal, at $T = 0.1 \text{ GeV}$ and various rapidities. Among them, the black line represents $\eta = 0.3$; the red dashed line represents $\eta = 0.6$.

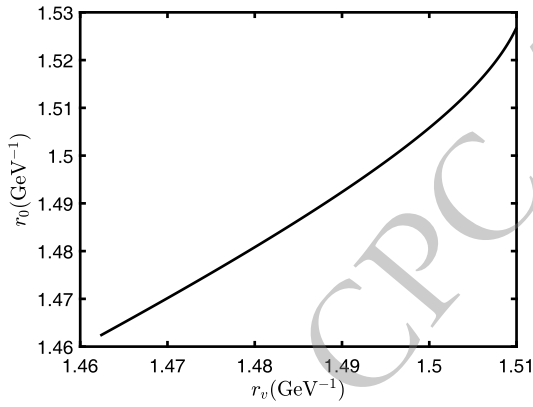


Fig. 8. (color online) The relation between the smooth turning point r_0 on the string and the position r_v of the baryon vertex at $T = 0.1 \text{ GeV}$, $\eta = 0.3$.

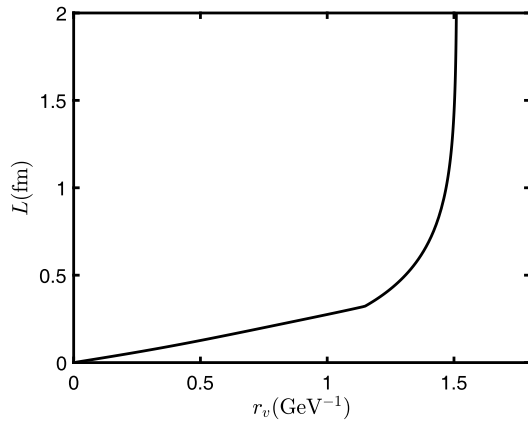


Fig. 9. (color online) The separation distance L between pairs of heavy quarks as a function of the position r_v of baryon vertex at $T = 0.1 \text{ GeV}$, $\eta = 0.3$.

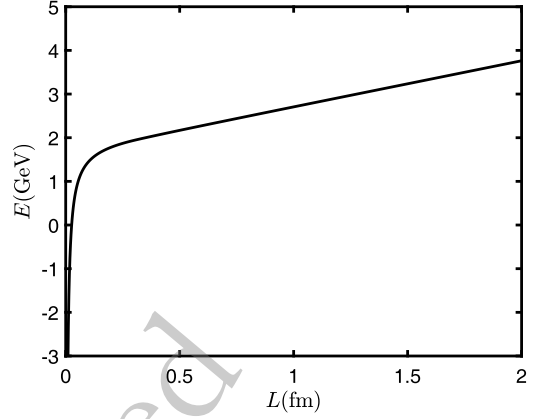
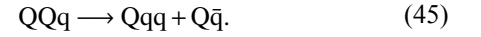


Fig. 10. (color online) The relation between QQq potential energy E and heavy-quark pair separation distance L at $T = 0.1 \text{ GeV}$, $\eta = 0.3$.

A. Confined state

When the QQq is confined, string breaking occurs when potential energy E reaches a certain value, exciting positive and negative light quarks in the vacuum. The pattern of string breaking is as follows:



The schematic diagram after the string breaking is [Fig. 11](#). It can be seen that the action of Qqq is provided by three strings, one baryon vertex, and two light quarks. The action of $\text{Q}\bar{q}$ consists of a string and a light quark. Therefore, the total action after the string breaking is:

$$S_{\text{Qqq}} = \sum_{i=1}^3 S_{\text{NG}}^{(i)} + S_{\text{vert}} + 2S_q, \quad (46)$$

$$S_{\text{Q}\bar{q}} = S_{\text{NG}} + S_q. \quad (47)$$

We choose the gauge as $\xi^0 = t$, $\xi^1 = r$, therefore, we obtain that the boundary condition of $x(r)$ is

$$(\partial_r x)^2 = 0. \quad (48)$$

So the total action can be written as

$$\begin{aligned} S = & gt \left(\int_0^{r_v} w(r) \sqrt{g_2(r)} dr + 2 \int_{r_v}^{r_q} w(r) \sqrt{g_2(r)} dr \right. \\ & \left. + \int_0^{r_q} w(r) \sqrt{g_2(r)} dr \right. \\ & \left. + 3k \frac{e^{-2sr_v^2}}{r_v} \sqrt{g_1(r_v)} + 3n \frac{e^{-\frac{sr_q^2}{2}}}{r_q} \sqrt{g_1(r_q)} \right). \end{aligned} \quad (49)$$

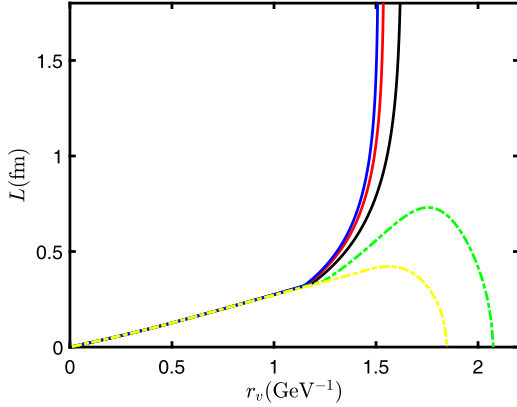


Fig. 13. (color online) The separation distance L between pairs of heavy quarks as a function of the position r_v of the baryon vertex at $T = 0.1 \text{ GeV}$. The solid line represents in confined state, while the dashed line represents in deconfined state. The blue line represents $\eta = 0.3$; the red line represents $\eta = 0.6$; the black line represents $\eta = 0.9$; the green line represents $\eta = 1.2$, and the yellow line represents $\eta = 1.3865$.

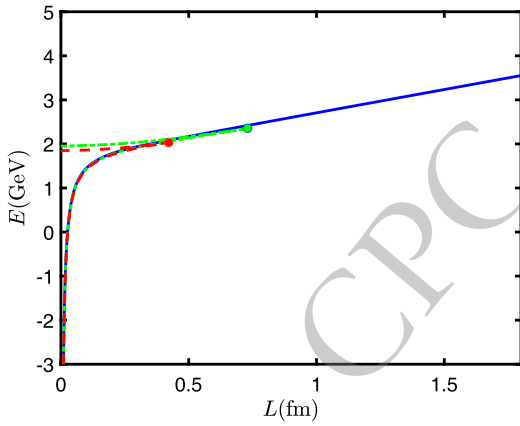


Fig. 14. (color online) The relation between the potential energy E and the separation distance L at $T = 0.1 \text{ GeV}$. The solid line represents in confined state, while the dashed line represents in deconfined state. The solid blue line represents $\eta = 0.3$; the green dot-dashed line represents $\eta = 1.2$; the red dashed line represents $\eta = 1.3865$.

the potential energy of the deconfined state. When E reaches the maximum value, L also reaches the maximum value, which is the apex of the L in Fig. 13. As the rapidity increases, the potential energy of QQq decreases, and the screening distance becomes smaller. Fig. 14 also illustrates that, regardless of whether it is in the confined or deconfined state, as the rapidity increases at a fixed temperature, the potential energy becomes smaller. The calculation results about the screening of the QQq in the deconfined state are as follows: at $\eta = 1.2$, $L_{\text{screen}} = 0.7304 \text{ fm}$, $E_{\text{screen}} = 2.3547 \text{ GeV}$; at $\eta = 1.3865$, $L_{\text{screen}} = 0.4219 \text{ fm}$, $E_{\text{screen}} = 2.0317 \text{ GeV}$.

We will briefly introduce the way used to determine

the confined and deconfined state. If the maximum value of the screening distance is smaller than the distance of string breaking, it indicates that the QQq is in the deconfined state; otherwise, it is in the confined state. Using this method, we perform calculations to determine the critical points, and these results are plotted in Fig. 15.

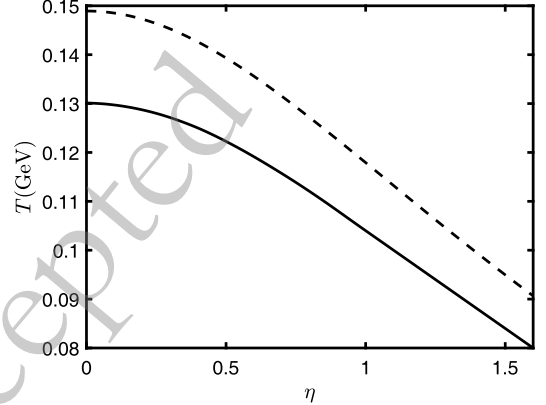


Fig. 15. (color online) The dashed line consists of the maximum (η, T) points determined by the Eqs. (44), and the solid line consists of the critical points that distinguish the confined state from the deconfined state.

In Fig. 15, QQq cannot exist in a medium with temperatures and rapidities above the dashed line. The QQq is in the deconfined state between the dashed and solid lines. In this state, QQq become free quarks at long distances due to screening. When QQq is in the deconfined state, with the increase of the rapidity at a fixed temperature, the screening distance decreases. Below the solid line, the QQq is in the confined state. In this state, when the separation distance reaches the string-breaking distance and string breaking occurs, it transitions into a new configuration.

C. Comparison with $Q\bar{Q}$ configuration

Research on $Q\bar{Q}$ through holographic models is mature enough [46, 62–69]. We mainly study the difference between $Q\bar{Q}$ and QQq under the influence of rapidities.

First of all, we can write the metric after adding the rapidity effect of $Q\bar{Q}$ through the Lorentz transformation:

$$ds^2 = w(r) \left(-g_1(r) dt^2 - 2 \sinh(\eta) \cosh(\eta) \left(1 - \frac{g_1(r)}{g_2(r)} \right) dx_3 dt + g_3(r) dx_3^2 + dx_1^2 + dx_2^2 + \frac{g_2(r)}{g_1(r)} dr^2 \right), \quad (52)$$

where $w(r)$, $g_1(r)$, $g_2(r)$, and $g_3(r)$ are consistent with the previously derived Eqs. (2) and (5).

We select the static gauge $\xi^0 = t$, $\xi^1 = x$, and the action of $Q\bar{Q}$ can be written as

$$S = gt \left(\int_{-\frac{L}{2}}^0 w(r) \sqrt{g_1(r) + g_2(r)(\partial_x r)^2} dx + \int_0^{\frac{L}{2}} w(r) \sqrt{g_1(r) + g_2(r)(\partial_x r)^2} dx \right). \quad (53)$$

And now the boundary condition of $r(x)$ is

$$r\left(\pm \frac{L}{2}\right) = 0, r(0) = r_0, (\partial_x r|_{r=r_0})^2 = 0. \quad (54)$$

The string configuration of $Q\bar{Q}$ is U-shaped, where r_0 is the smooth turning point of the U-shaped string. With the Euler Lagrange equation, we can obtain

$$\partial_x r = \sqrt{\frac{w(r)^2 g_1(r)^2 - g_1(r) w(r_0)^2 g_1(r_0)}{w(r_0)^2 g_1(r_0) g_2(r)}}. \quad (55)$$

By renormalizing, we can obtain the potential energy of $Q\bar{Q}$,

$$E_{Q\bar{Q}} = g \left(2 \int_0^{r_0} (w(r) \sqrt{g_1(r)(\partial_x r)^2 + g_2(r)} - \frac{1}{r^2}) dr - \frac{2}{r_0} \right) + 2c. \quad (56)$$

And,

$$L = 2 \int_0^{r_0} \frac{\partial x}{\partial r} dr, \quad (57)$$

where $\partial_x r = \frac{\partial x}{\partial r} = \frac{1}{\partial_x r}$.

We can calculate the potential energy of $Q\bar{Q}$ at different rapidities at the same temperature and compare it with QQq . The result is presented in Fig. 16, indicating that the potential energy of QQq is higher than that of $Q\bar{Q}$. Furthermore, it is observed that increasing rapidity consistently leads to a decrease in the potential energy of $Q\bar{Q}$ and QQq . When $Q\bar{Q}$ is in the confined state, the $Q\bar{Q}$ string breaks when the separation distance becomes large enough. Let us consider the pattern of $Q\bar{Q}$ string breaking as

$$Q\bar{Q} \longrightarrow Q\bar{q} + \bar{Q}q. \quad (58)$$

It is easy to know that

$$E_{break} = 2g \left(\int_0^{r_q} (w(r) \sqrt{g_2(r)} - \frac{1}{r^2}) dr - \frac{1}{r_q} + n \frac{e^{\frac{sr_q^2}{2}}}{r_q} \sqrt{g_1(r_q)} \right) + 2c. \quad (59)$$

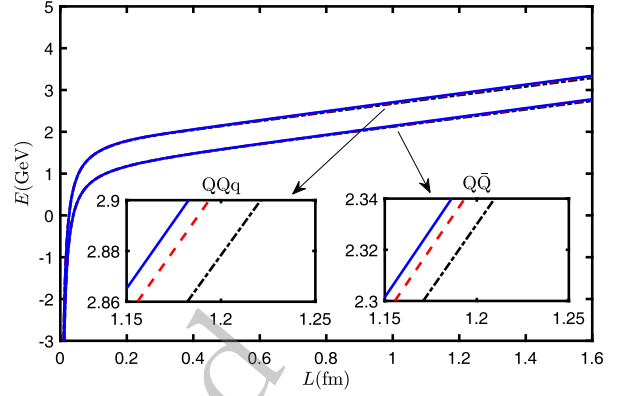


Fig. 16. (color online) The potential energies of $Q\bar{Q}$ and QQq are depicted at $T = 0.1$ GeV. In the graph, the black dot-dashed line represents $\eta = 0.9$; the red dashed line represents $\eta = 0.6$; and the blue solid line represents $\eta = 0.3$.

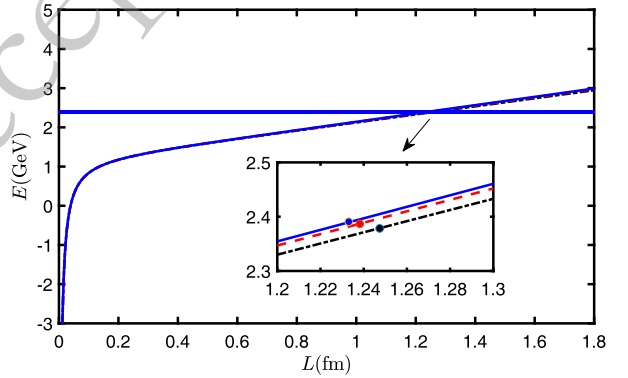


Fig. 17. (color online) The curves in the figure are the potential energy of $Q\bar{Q}$ at $T = 0.1$ GeV, and the straight lines are the potential energy at $T = 0.1$ GeV after string breaking. Where the black dot-dashed line represents $\eta = 0.9$; the red dashed line represents $\eta = 0.6$; and the blue solid line represents $\eta = 0.3$.

Based on this, we can draw Fig. 17. As shown in the figure, it is evident that increasing rapidity leads to a greater separation distance at the point of string breaking for both $Q\bar{Q}$ and QQq . The calculated data are $\eta = 0.3$, $E_{break} = 2.3906$ GeV, $L_{break} = 1.2331$ fm; $\eta = 0.6$, $E_{break} = 2.3868$ GeV, $L_{break} = 1.2382$ fm; $\eta = 0.9$, $E_{break} = 2.3784$ GeV, $L_{break} = 1.2474$ fm. It can be observed that the breaking distance of $Q\bar{Q}$ is slightly less than QQq , but the difference between the two is not significant.

When the rapidity continues to increase, $Q\bar{Q}$ will also change from the confined state to the deconfined state. For this purpose, we calculated the results in Fig. 18. When we calculated the potential of QQq at $\eta = 1.3865$ and $T = 0.1$ GeV, the results show $L_{melt} = 0.4219$ fm and $E_{melt} = 2.0317$ GeV. When $Q\bar{Q}$ is at $\eta = 1.3865$ and $T = 0.1$ GeV, we get $L_{melt} = 0.8944$ fm and $E_{melt} = 1.9640$ GeV. It can be found that the difference in screening distances is significant. We infer that $Q\bar{Q}$ is

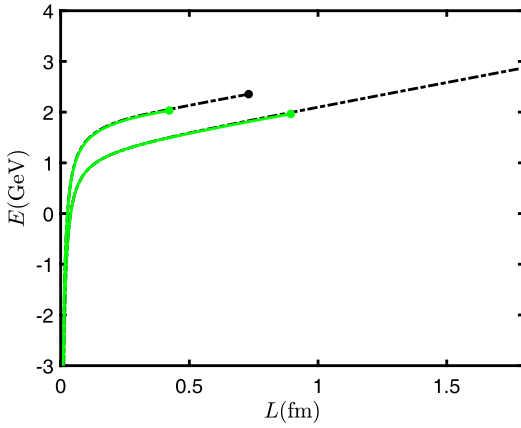


Fig. 18. (color online) The higher curves represent QQq, and the lower curves represent $Q\bar{Q}$. The black line represents $\eta = 1.2$, $T = 0.1$ GeV, and the green line represents $\eta = 1.3865$, $T = 0.1$ GeV.

more stable than QQq at the same temperature and rapidity.

Fig. 19 shows QQq is confined below the black line, which means the separation distance of heavy quarks can be infinite if we ignore the string breaking. QQq can still be found below the black dashed line even the QQq is in the deconfined state which means the QQq can screen at a certain distance. QQq can not be found anymore above the dashed line. As a comparison, we show $Q\bar{Q}$ in the same figure with a blue line. The situation is different for $Q\bar{Q}$. The $Q\bar{Q}$ is confined below the blue line. Above the blue line, $Q\bar{Q}$ is deconfined; however, we can still find the $Q\bar{Q}$ at any conditions since it can still exist at a small separation distance.

IV. CONCLUSION

In this paper, we mainly discuss the properties of QQq in some aspects at finite temperature and rapidity using the 5-dimensional effective string model for the first time. When the QQq is in the confined state, it can undergo string breaking at a large separation distance. We consider the breaking mode to be $QQq \rightarrow Qq + Q\bar{q}$ and observe that higher rapidities make the string breaking more difficult to occur. Under high temperature and

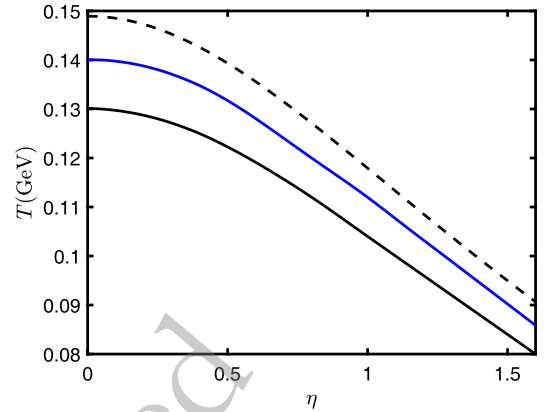


Fig. 19. (color online) The solid black line is to distinguish the confined state and the deconfined state of QQq; the dashed line is the maximum conditions allowed by QQq; the blue line is to distinguish the confined state and the deconfined state of $Q\bar{Q}$.

rapidity conditions, the QQq transitions into the deconfined state. In this state, it becomes the free quarks if the separation distance is larger than the screening distance, and color screening becomes easier with increasing rapidity. Using potential analysis, we constructed a state diagram for QQq in the $T - \eta$ plane to differentiate between the confined and deconfined states.

We compared the properties of QQq and $Q\bar{Q}$. As expected, the potential energy of QQq is always greater than that of $Q\bar{Q}$, and the qualitative effects of temperature and rapidity on QQq and $Q\bar{Q}$ are consistent. In the confined state, it is found that the string-breaking distance of QQq and $Q\bar{Q}$ are very close. In other words, it may show the size of the different hadrons are similar. In the deconfined state, there is a significant difference in the screening distance between QQq and $Q\bar{Q}$. It is found that the screening distance of QQq is smaller than that of $Q\bar{Q}$ under the same conditions, which indicates QQq is less stable than $Q\bar{Q}$. Besides, an interesting result shows that QQq cannot be found above certain temperatures and rapidities. However, $Q\bar{Q}$ can be found at any temperature and rapidity as long as the separation distances are small enough. This work mainly focuses on qualitative analysis and can be extended to yield more accurate results in the future.

References

- [1] R. Aaij *et al.*[LHCb], *Phys. Rev. Lett.* **119**(11), 112001 (2017), arXiv:1707.01621[hep-ex]
- [2] R. Aaij *et al.*[LHCb], *Phys. Rev. Lett.* **121**(16), 162002 (2018), arXiv:1807.01919[hep-ex]
- [3] E. Eichten, K. Gottfried, T. Kinoshita, K. D. Lane and T. M. Yan, *Phys. Rev. D* **21**, 203 (1980)
- [4] A. Yamamoto, H. Suganuma and H. Iida, *Phys. Rev. D* **78**, 014513 (2008), arXiv:0806.3554[hep-lat]
- [5] J. Najjar and G. Bali, *PoS LAT2009*, 089 (2009), arXiv:0910.2824[hep-lat]
- [6] J. M. Maldacena, *Phys. Rev. Lett.* **80**, 4859 (1998), arXiv:hep-th/9803002[hep-th]
- [7] S. J. Rey, S. Theisen and J. T. Yee, *Nucl. Phys. B* **527**, 171 (1998), arXiv:hep-th/9803135[hep-th]
- [8] A. Brandhuber, N. Itzhaki, J. Sonnenschein and S. Yankielowicz, *Phys. Lett. B* **434**, 36 (1998), arXiv:hep-th/9803137[hep-th]

- [9] C. Alexandrou, P. de Forcrand and O. Jahn, *Nucl. Phys. B Proc. Suppl.* **119**, 667 (2003), arXiv:hep-lat/0209062[hep-lat]
- [10] C. Alexandrou, P. De Forcrand and A. Tsapalis, *Nucl. Phys. B Proc. Suppl.* **106**, 403 (2002), arXiv:hep-lat/0110115[hep-lat]
- [11] T. T. Takahashi, H. Suganuma, Y. Nemoto and H. Matsufuru, *Phys. Rev. D* **65**, 114509 (2002), arXiv:hep-lat/0204011[hep-lat]
- [12] O. Andreev, *JHEP* **05**, 173 (2021), arXiv:2007.15466[hep-ph]
- [13] O. Andreev, *Phys. Lett. B* **756**, 6 (2016), arXiv:1505.01067[hep-ph]
- [14] O. Andreev, *Phys. Rev. D* **93**(10), 105014 (2016), arXiv:1511.03484[hep-ph]
- [15] O. Andreev, *Phys. Rev. D* **107**(2), 026023 (2023), arXiv:2211.12305[hep-ph]
- [16] O. Andreev, *Phys. Rev. D* **106**(6), 066002 (2022), arXiv:2205.12119[hep-ph]
- [17] O. Andreev, *Phys. Rev. D* **108**(10), 106012 (2023), arXiv:2306.08581[hep-ph]
- [18] O. Andreev, *Phys. Rev. D* **105**(8), 086025 (2022), arXiv:2111.14418[hep-ph]
- [19] O. Andreev, *Phys. Lett. B* **804**, 135406 (2020), arXiv:1909.12771[hep-ph]
- [20] O. Andreev, *Phys. Rev. D* **104**(2), 026005 (2021), arXiv:2101.03858[hep-ph]
- [21] A. Yamamoto, H. Suganuma and H. Iida, *Prog. Theor. Phys. Suppl.* **174**, 270 (2008), arXiv:0805.4735[hep-ph]
- [22] M. Laine, *PoS LAT2006*, 014 (2006), arXiv:hep-lat/0612023[hep-lat]
- [23] T. Asaka, M. Laine and M. Shaposhnikov, *JHEP* **06**, 053 (2006), arXiv:hep-ph/0605209[hep-ph]
- [24] M. Hindmarsh and O. Philipsen, *Phys. Rev. D* **71**, 087302 (2005), arXiv:hep-ph/0501232[hep-ph]
- [25] A. Rothkopf, *Phys. Rept.* **858**, 1 (2020), arXiv:1912.02253[hep-ph]
- [26] T. Matsui and H. Satz, *Phys. Lett. B* **178**, 416 (1986)
- [27] D. Kharzeev and H. Satz, doi: 10.1142/9789812830661_0007[arXiv:hep-ph/9505345[hep-ph]].
- [28] E. Witten, *Adv. Theor. Math. Phys.* **2**, 505 (1998), arXiv:hep-th/9803131[hep-th]
- [29] F. Bigazzi, A. L. Cotrone, L. Martucci and W. Troost, *Fortsch. Phys.* **55**, 666 (2007), arXiv:hep-th/0611253[hep-th]
- [30] J. M. Maldacena, *Adv. Theor. Math. Phys.* **2**, 231 (1998), arXiv:hep-th/9711200[hep-th]
- [31] O. Aharony, S. S. Gubser, J. M. Maldacena, H. Ooguri and Y. Oz, *Phys. Rept.* **323**, 183 (2000), arXiv:hep-th/9905111[hep-th]
- [32] J. Casalderrey-Solana, H. Liu, D. Mateos, K. Rajagopal and U. A. Wiedemann, Cambridge University Press, 2014, ISBN 978-1-139-13674-7 doi: 10.1017/CBO9781139136747 [arXiv:1101.0618[hep-th]].
- [33] S. S. Gubser, *Found. Phys.* **43**, 140 (2013), arXiv:1103.3636[hep-th]
- [34] H. Liu, K. Rajagopal and U. A. Wiedemann, *Phys. Rev. Lett.* **98**, 182301 (2007), arXiv:hep-ph/0607062[hep-ph]
- [35] S. I. Finazzo and J. Noronha, *JHEP* **01**, 051 (2015), arXiv:1406.2683[hep-th]
- [36] L. Thakur, N. Haque and H. Mishra, *Phys. Rev. D* **95**(3), 036014 (2017), arXiv:1611.04568[hep-ph]
- [37] J. Zhou, X. Chen, Y. Q. Zhao and J. Ping, *Phys. Rev. D* **102**(8), 086020 (2020), arXiv:2006.09062[hep-ph]
- [38] S. Q. Feng, Y. Q. Zhao and X. Chen, *Phys. Rev. D* **101**(2), 026023 (2020), arXiv:1910.05668[hep-ph]
- [39] J. Zhou, X. Chen, Y. Q. Zhao and J. Ping, *Phys. Rev. D* **102**(12), 126029 (2021)
- [40] K. Bitaghsir Fadafan and S. K. Tabatabaei, *J. Phys. G* **43**(9), 095001 (2016), arXiv:1501.00439[hep-th]
- [41] M. A. Escobedo, F. Giannuzzi, M. Mannarelli and J. Soto, *Phys. Rev. D* **87**(11), 114005 (2013), arXiv:1304.4087[hep-ph]
- [42] X. Chen, L. Zhang, D. Li, D. Hou and M. Huang, *JHEP* **07**, 132 (2021), arXiv:2010.14478[hep-ph]
- [43] X. Chen, S. Q. Feng, Y. F. Shi and Y. Zhong, *Phys. Rev. D* **97**(6), 066015 (2018), arXiv:1710.00465[hep-ph]
- [44] T. Song, Y. Park, S. H. Lee and C. Y. Wong, *Phys. Lett. B* **659**, 621 (2008), arXiv:0709.0794[hep-ph]
- [45] M. Ali-Akbari, D. Giataganas and Z. Rezaei, *Phys. Rev. D* **90**(8), 086001 (2014), arXiv:1406.1994[hep-th]
- [46] O. Andreev, *Nucl. Phys. B* **977**, 115724 (2022), arXiv:2106.14716[hep-ph]
- [47] C. Krishnan, *JHEP* **12**, 019 (2008), arXiv:0809.5143[hep-th]
- [48] X. Yao and T. Mehen, *JHEP* **02**, 062 (2021), arXiv:2009.02408[hep-ph]
- [49] M. Chermicoff, D. Fernandez, D. Mateos and D. Trancanelli, *JHEP* **01**, 170 (2013), arXiv:1208.2672[hep-th]
- [50] S. C. Benzahra, *Afr. J. Math. Phys.* **1**, 191 (2004)
- [51] O. Andreev, *Phys. Lett. B* **659**, 416 (2008), arXiv:0709.4395[hep-ph]
- [52] X. Chen, B. Yu, P. C. Chu and X. h. Li, *Chin. Phys. C* **46**(7), 073102 (2022), arXiv:2112.06234[hep-ph]
- [53] O. Andreev, *Phys. Rev. D* **76**, 087702 (2007), arXiv:0706.3120[hep-ph]
- [54] E. Witten, *JHEP* **02**, 006 (1998), arXiv:hep-th/9712028[hep-th]
- [55] S. Gukov, M. Rangamani and E. Witten, *JHEP* **12**, 025 (1998), arXiv:hep-th/9811048[hep-th]
- [56] O. Andreev, *Phys. Rev. D* **101**(10), 106003 (2020), arXiv:2003.09880[hep-ph]
- [57] J. Erlich, E. Katz, D. T. Son and M. A. Stephanov, *Phys. Rev. Lett.* **95**, 261602 (2005), arXiv:hep-ph/0501128[hep-ph]
- [58] X. Cao, M. Baggioli, H. Liu and D. Li, *JHEP* **12**, 113 (2022), arXiv:2210.09088[hep-ph]
- [59] X. Cao, J. Chao, H. Liu and D. Li, *Phys. Rev. D* **107**(8), 086001 (2023), arXiv:2204.11604[hep-ph]
- [60] Y. Yang and P. H. Yuan, *JHEP* **12**, 161 (2015), arXiv:1506.05930[hep-th]
- [61] O. Andreev and V. I. Zakharov, *JHEP* **04**, 100 (2007), arXiv:hep-ph/0611304[hep-ph]
- [62] P. Colangelo, F. Giannuzzi and S. Nicotri, *Phys. Rev. D* **83**, 035015 (2011), arXiv:1008.3116[hep-ph]
- [63] O. Andreev and V. I. Zakharov, *Phys. Lett. B* **645**, 437 (2007), arXiv:hep-ph/0607026[hep-ph]
- [64] C. Ewerz, O. Kaczmarek and A. Samberg, *JHEP* **03**, 088 (2018), arXiv:1605.07181[hep-th]
- [65] S. He, M. Huang and Q. s. Yan, *Prog. Theor. Phys. Suppl.* **186**, 504 (2010), arXiv:1007.0088[hep-ph]
- [66] D. Li, S. He, M. Huang and Q. S. Yan, *JHEP* **09**, 041 (2011), arXiv:1103.5389[hep-th]
- [67] K. B. Fadafan, *Eur. Phys. J. C* **71**, 1799 (2011), arXiv:1102.2289[hep-th]
- [68] K. B. Fadafan and E. Azimfard, *Nucl. Phys. B* **863**, 347 (2012), arXiv:1203.3942[hep-th]
- [69] R. G. Cai, S. He and D. Li, *JHEP* **03**, 033 (2012), arXiv:1201.0820[hep-th]